Article

Formation of Monodisperse and Shape-Controlled MnO Nanocrystals in Non-Injection Synthesis: Self-Focusing via Ripening

Yongfen Chen, Eric Johnson, and Xiaogang Peng

J. Am. Chem. Soc., **2007**, 129 (35), 10937-10947• DOI: 10.1021/ja073023n • Publication Date (Web): 14 August 2007

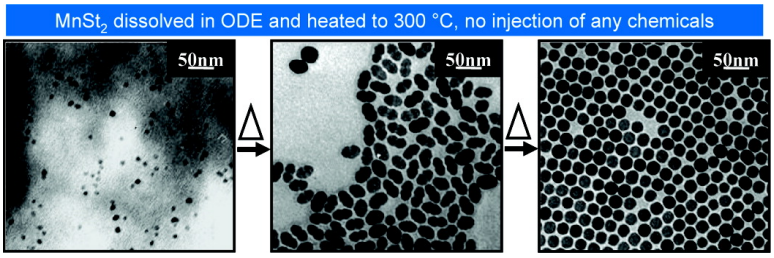

More About This Article

Additional resources and features associated with this article are available within the HTML version:

- Supporting Information
- Links to the 9 articles that cite this article, as of the time of this article download
- Access to high resolution figures
- Links to articles and content related to this article
- Copyright permission to reproduce figures and/or text from this article

View the Full Text HTML

J|A|C|S
ARTICLES
Published on Web 08/14/2007

Formation of Monodisperse and Shape-Controlled MnO Nanocrystals in Non-Injection Synthesis: Self-Focusing via Ripening

Yongfen Chen, Eric Johnson, and Xiaogang Peng*

Contribution from the Department of Chemistry & Biochemistry, University of Arkansas, Fayetteville, Arkansas 72701

Received April 30, 2007; E-mail: xpeng@uark.edu

Abstract: Formation of nearly monodiperse MnO nanocrystals by simple heating of Mn stearate in octadecene was studied systematically and quantitatively as a model for non-injection synthesis of nanocrystals. For controlling the shape of the nanocrystals, that is, rice, rods, peanuts, needles, and dots, either an activation reagent (ocadecanol) or an inhibitor (stearic acid) might be added prior to heating. The quantitative results of this typical non-injection system reveal that the formation of nearly monodisperse nanocrystals did not follow the well-known "focusing of size distribution" mechanism. A new growth mechanism, self-focusing enabled by inter-particle diffusion, is proposed. Different from the traditional "focusing of size distribution", self-focusing not only affects the growth process of the nanocrystals, but may also play a role in controlling nucleation. Because of the simplicity of the reaction system, it was possible to also identify the chemical reactions associated with the growth and ripening of MnO nanocrystals with a variety of shapes. Through a recycling reaction path, water was identified as a decisive component in determining the kinetics for both growth and ripening in this system, although the reaction occurred at around 300 °C.

Introduction

Formation of monodisperse nanocrystals with size and shape control has recently become a central topic in the field of materials chemistry.[1,2] This topic not only represents a synthetic challenge, but also is of importance in several areas of science, such as optoelectronics,[3,4] bio-medical sensing,[5,6] catalysis,[7] crystallization,[8] and natural/bio-mineralization,[9] etc. For this topic, one established concept, "focusing of size distribution",[10] has played a key role. Hot-injection methods, initiating reaction by the injection of cold precursors into a hot solvent, are specifically based on this concept and have become the mainstream approach in the synthesis of nearly monodisperse nanocrystals.[1,2] By experimental design, nucleation stops shortly after the injection because of the subsequent decrease of monomer concentration and reaction temperature. If the remaining monomer concentration is higher than the solubility of all nanocrystals in the system, "focusing of size distribution" occurs in this net growth stage because the growth rate of nanocrystals increases as their size decreases.[2,10] Interestingly, some recent reports indicate that hot injections may not be needed at all. Nearly monodisperse nanocrystals, including oxides,[11−14] II−VI semiconductor nanocrystals,[15,16] and noble metal ones,[17−19] can be obtained more or less by simply heating up all premixed reactants. Such simple non-injection-based synthesis may be widely exploited if the mechanism on controlling the size and size distribution of the nanocrystals can be well understood. This along with the general importance of understanding crystallization mentioned above was the motivation of this work.

Growth of MnO nanocrystals by simply heating Mn stearate in a hydrocarbon solvent, sometimes with either some free stearic acid as the inhibitor or ocadecanol as the activation reagent, was chosen as our model system. MnO nanocrystals are probably the most studied oxide nanocrystal system in the recent literature, especially in terms of shape control.[13,14,20−26]

(1) Murray, C. B.; Kagan, C. R.; Bawendi, M. G. *Annu. Rev. Mater. Sci.* **2000**, *30*, 545−610.
(2) Peng, X.; Thessing, J. *Struct. Bonding* **2005**, *118*, 79−119.
(3) Colvin, V. L.; Schlamp, M. C.; Allvisatos, A. P. *Nature* **1994**, *370*, 354−7.
(4) Greenham, N. C.; Peng, X.; Alivisatos, A. P. *Phys. Rev. B: Condens. Matter* **1996**, *54*, 17628−17637.
(5) Bruchez, M., Jr.; Moronne, M.; Gin, P.; Weiss, S.; Alivisatos, A. P. *Science* **1998**, *281*, 2013−2016.
(6) Chan, W. C. W.; Nile, S. *Science* **1998**, *281*, 2016−2018.
(7) For example: Dong, W.; Cogbill, A.; Zhang, T.; Ghosh, S.; Tian, Z. R. *J. Phys. Chem. B* **2006**, *110*, 16819−16822.
(8) Peng, Z. A.; Peng, X. *J. Am. Chem. Soc.* **2002**, *124*, 3343−3353.
(9) Penn, R. L.; Banfield, J. F. *Science* **1998**, *281*, 969−971.
(10) Peng, X.; Wickham, J.; Alivisatos, A. P. *J. Am. Chem. Soc.* **1998**, *120*, 5343−5344.
(11) Hyeon, T.; Lee, S. S.; Park, J.; Chung, Y.; Na, H. B. *J. Am. Chem. Soc.* **2001**, *123*, 12798−12801.
(12) Sun, S.; Zeng, H. *J. Am. Chem. Soc.* **2002**, *124*, 8204−8205.
(13) Yin, M.; O'Brien, S. *J. Am. Chem. Soc.* **2003**, *125*, 10180−10181.
(14) Jana, N. R.; Chen, Y.; Peng, X. *Chem. Mater.* **2004**, *16*, 3931−3935.
(15) Joo, J.; Na, H. B.; Yu, T.; Yu, J. H.; Kim, Y. W.; Wu, F.; Zhang, J. Z.; Hyeon, T. *J. Am. Chem. Soc.* **2003**, *125*, 11100−11105.
(16) Yang, Y. A.; Wu, H.; Williams, K. R.; Cao, Y. C. *Angew. Chem., Int. Ed.* **2005**, *44*, 6712−6715.
(17) Stoeva, S.; Klabunde, K. J.; Sorensen, C. M.; Dragieva, I. *J. Am. Chem. Soc.* **2002**, *124*, 2305−2311.
(18) Jana, N. R.; Peng, X. *J. Am. Chem. Soc.* **2003**, *125*, 14280−14281.
(19) Hiramatsu, H.; Osterloh, F. E. *Chem. Mater.* **2004**, *16*, 2509−2511.
(20) Ahmad, T.; Ramanujachary, K. V.; Lofland, S. E.; Ganguli, A. K. *J. Mater. Chem.* **2004**, *14*, 3406−3410.
(21) Park, J.; Kang, E.; Bae, C. J.; Park, J.-G.; Noh, H.-J.; Kim, J.-Y.; Park, J.-H.; Park, H. M.; Hyeon, T. *J. Phys. Chem. B* **2004**, *108*, 13594−13598.

The simplicity of our model system made it relatively easy to follow the reactants and products along the formation of the oxide nanocrystals as to be discussed below. Furthermore, similar reaction systems were studied for the formation of high-quality ZnO and In_2O_3 nanocrystals using hot-injection methods.[27,28] However, the purpose of this work required the study to be at a quantitative level as to be described below. In contrast, the studies on hot-injection synthesis of ZnO and In_2O_3 nanocrystals were qualitative.[27,28]

The well-studied II−VI and III−V semiconductor nanocrystal systems can be conveniently probed using their size-dependent optical properties with an accuracy down to a few atoms.[29] MnO nanocrystals, similar to most oxide nanocrystals, do not have strong size-dependent optical properties. To solve this problem, this work explored possibilities to use FTIR coupled with a transmission electron microscope (TEM) as quantitative probes. Because of the chosen reaction system, FTIR allowed direct measurements of the concentrations of the precursor and the organic side products in the reaction solution. It should be pointed out that application of FTIR measurements in monitoring nanocrystal synthesis has already been well demonstrated qualitatively in the literature.[30] In addition to FTIR, quantitative analysis of TEM images of the nanocrystals offered information on the size, shape, and size/shape distribution of the nanocrystals. Combining the information from TEM and FTIR measurements, one can calculate the particle concentration in the solution. Thus, the crystallization system can be well defined. This approach, presumably working for different types of nanocrystals, is less accurate in terms of determining the size of the nanocrystals in comparison to the existing approaches developed for studying formation of semiconductor nanocrystals using their size-dependent optical properties. However, it may offer significantly more information about the molecular mechanisms for a carefully designed system that could be fully followed by FTIR spectroscopy. As will be described later, this advantage was further utilized to directly verify a long standing hypothesis that the reactivity of monomers can be tuned by the addition of free ligands, which was repeatedly implied by the growth kinetics of different types of semiconductor nanocrystals.[31−33]

The results to be discussed below suggested that formation of monodispserse MnO nanocrystals in this non-injection-based system was unlikely a traditional "focusing of size distribution" process. Different from one typical feature of the "focusing of size distribution" process described above, the particle concentration in the current system was found to decrease significantly when the size distribution was narrowed down. It should be mentioned that a substantial decrease of particle concentration was also observed previously for the formation of CdSe nanocrystals in a non-injection approach,[16] which is probably the only publication reporting the particle concentration evolution for non-injection synthesis of nanocrystals. Some further contradictions to the "focusing of size distribution" model are also identified. For instance, the consumption of monomers was found to be close to zero in the main duration of the size-focusing process for the current system.

A new mechanism, self-focusing, will be proposed. This mechanism is based on inter-particle diffusion observed recently,[34] which allows a rapid and complete dissolution of the small particles in the system. This means that, while the size distribution is narrowed down in this transient stage of Oswald ripening, the particle concentration shall decrease. Different from the traditional "focusing of size distribution", self-focusing requires a high particle concentration in the solution but does not depend on a high monomer concentration. Unlike the traditional "focusing of size distribution", self-focusing might also affect the nucleation process in a system.

In addition to the growth mechanism of the nanocrystals, this work also studied the chemical reactions involved in the formation of nearly monodipserse MnO nanocrystals with a variety of shapes. The identified reaction mechanism was found to be different from the molecular mechanisms of either the ZnO nanocrystal system or In_2O_3 reported previously.[27,28] The main interesting finding on this aspect is that water was confirmed to play a key role in both growth and ripening of the MnO nanocrystals in the current system. Although the emphasis of this Article is on the formation of nearly monodisperse dot-shaped nanocrystals, some aspects related to shape control of high-quality nanocrystals will also be briefly described.

Results

The model reaction system chosen for studying non-injection synthesis of high-quality nanocrystals was the formation of MnO nanocrystals in non-coordinating solvents under elevated temperatures,[14] with Mn stearate ($MnSt_2$) as the sole precursor and ocadecene (ODE) as the non-coordinating solvent. If needed, free stearic acid (HSt) was used as inhibitor and octadecanol was applied as activation reagents. Different from the two oxide nanocrystal systems studied previously, ZnO[27] and In_2O_3,[28] no hot-injection of any chemicals was applied in the current system, and, as pointed out above, the current system would be quantitatively defined, instead of being at a qualitative level for the two existing examples based on hot injections.

FTIR spectra of the aliquots taken at different reaction time intervals were recorded, and the vibration peaks at 1556, 1740, and 1700−1720 cm^{-1} are assigned as the carbonyl vibration bands of carboxylate salt, ester, and carboxylic acid, respectively.[35] The $-CH_3$ peak at 1375 cm^{-1} was found to be a good reference for quantitative calculations for reactions lasting for several hours.

Dot-shaped MnO nanocrystals were formed as the sole product in all duration of a growth reaction when ocadecanol

(22) Zitoun, D.; Pinna, N.; Frolet, N.; Belin, C. *J. Am. Chem. Soc.* **2005**, *127*, 15034−15035.
(23) Ghosh, M.; Biswas, K.; Sundaresan, A.; Rao, C. N. R. *J. Mater. Chem.* **2006**, *16*, 106−111.
(24) Ould-Ely, T.; Prieto-Centurion, D.; Kumar, A.; Guo, W.; Knowles, W. V.; Asokan, S.; Wong, M. S.; Rusakova, I.; Luettge, A.; Whitmire, K. H. *Chem. Mater.* **2006**, *18*, 1821−1829.
(25) Shanmugam, S.; Gedanken, A. *J. Phys. Chem. B* **2006**, *110*, 24486−24491.
(26) Zhong, X.; Xie, R.; Sun, L.; Lieberwirth, I.; Knoll, W. *J. Phys. Chem. B* **2006**, *110*, 2−4.
(27) Chen, Y.; Kim, M.; Lian, G.; Johnson, M. B.; Peng, X. *J. Am. Chem. Soc.* **2005**, *127*, 13331−13337.
(28) Narayanaswamy, A.; Xu, H.; Pradhan, N.; Kim, M.; Peng, X. *J. Am. Chem. Soc.* **2006**, *128*, 10310−10319.
(29) Brus, L. E. *J. Chem. Phys.* **1984**, *80*, 4403−9.
(30) For example: Zhang, Z.; Zhong, X.; Liu, S.; Li, D.; Han, M. *Angew. Chem., Int. Ed.* **2005**, *44*, 3466−3470.
(31) Yu, W. W.; Peng, X. *Angew. Chem., Int. Ed.* **2002**, *41*, 2368−2371.
(32) Battaglia, D.; Peng, X. *Nano Lett.* **2002**, *2*, 1027−1030.
(33) Yu, W. W.; Wang, Y. A.; Peng, X. *Chem. Mater.* **2003**, *15*, 4300−4308.
(34) Thessing, J.; Qian, J.; Chen, H.; Pradhan, N.; Peng, X. *J. Am. Chem. Soc.* **2007**, *129*, 2736−2737.
(35) Bellamy, L. J. *The Infra-Red Spectra of Complex Molecules*, 3rd ed.; Halsted: New York, 1975; 425 pp.

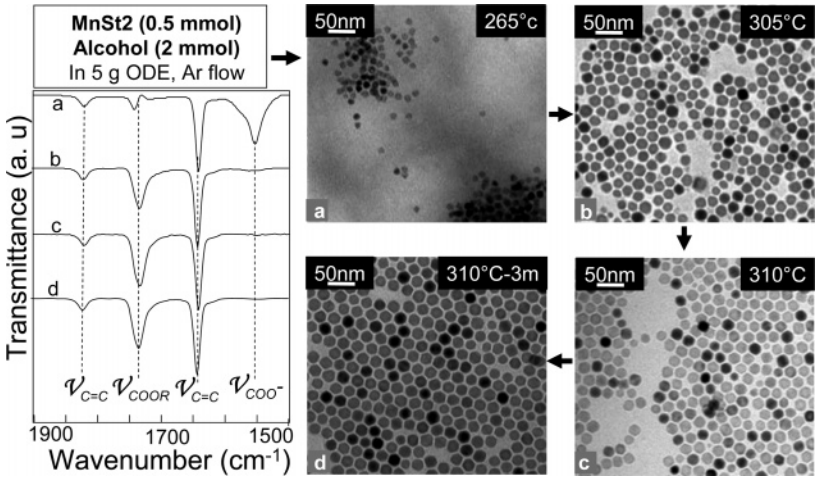

Figure 1. Temporal evolution of size and size distribution of MnO nanocrystals with alcohol (octadecanol) added as the activation reagents. The corresponding FTIR spectrum for each TEM image is provided on the left side with the vibrational bands for different groups marked.

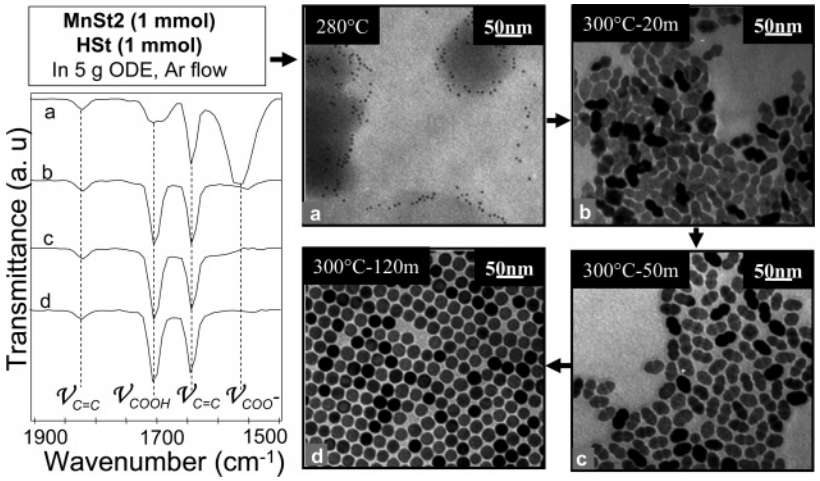

Figure 2. Temporal evolution of size and size distribution of MnO nanocrystals with free stearic acid (HSt) added as the inhibitors. The corresponding FTIR spectrum for each TEM image is provided on the left side with the vibrational bands for different groups marked.

was added as an activation reagent. The temporal evolution of TEM images and FTIR spectra for a typical reaction is shown in Figure 1. When the temperature was below about 250 °C, no particles were observed by TEM. At about 265 °C (Figure 1a), small MnO nanocrystals started to appear, and the sizes of the dots increased rapidly (Figure 1). After the temperature reached 310 °C for about 3 min, nearly monodisperse MnO nanocrystals were obtained (Figure 1d). By simply looking at the TEM images in Figure 1, one might have concluded that this was a typical process of "focusing of size distribution".

FTIR spectra (Figure 1, left), however, reveal a nearly complete depletion of the $MnSt_2$ precursor when the temperature reached 305 °C (Figure 1b). This means that, although narrowing of size distribution of the nanocrystals evidently occurred from the time corresponding to Figure 1b to the time corresponding to Figure 1d, the precursor was almost completely consumed prior to this focusing process. Along this focusing process, the average size showed a significant increase even without looking at the quantitative data to be described below. These features, growth and focusing without consuming a significant amount of monomers, imply that this process was different from the traditional "focusing of size distribution". As pointed out above, the traditional "focusing of size distribution" requires all particles grow simultaneously, and the simultaneous growth of all particles must consume a certain amount of monomers. Because the monomer concentration was close to zero from Figure 1b to Figure 1d, the monomers needed for the growth of the final monodisperse dots were likely from the nanocrystals themselves, which indicates a ripening process. The quantitative data to be described below will provide further evidence to support this conclusion.

Monodisperse spherical nanocrystals from elongated shapes can be obtained when elongated nanocrystals were formed in the early stage. Generally speaking, when activation reagents (alcohol) were not added, reactions yielded elongated MnO nanocrystals, ranging from rice-shape, peanut-shape, rod-shape, etc., in the early stage under the chosen reaction conditions for the current system. If the system was allowed to age for a sufficient amount of time, these elongated nanocrystals would be converted to dot-shaped. Figure 2 illustrates one of such reactions that converted nearly monodisperse peanuts (Figure 2b and c) to nearly monodisperse dots (Figure 2d). This reaction started with small sized dots (Figure 2a), and then these dots grew to relatively large peanuts (Figure 2b) within a matter of a few minutes (additional data in the Supporting Information, Figure S1). The initially formed peanuts (Figure 2b) were with sharp corners that were gradually smoothed out to form nearly monodisperse round peanuts (Figure 2c). This smoothing process

did not change the average volume of the nanocrystals noticeably. The FTIR spectra (Figure 2, left) indicate that precursors were nearly completely consumed when this smoothing process started. These features are consistent with an intra-particle ripening process.[36]

Further annealing of these peanuts converted the elongated nanocrystals into dots with a nearly monodisperse size distribution (Figure 2d). This process was noticed to be quite slow, over 1 h, and the shape transition was a gradual process (see additional data in Figure S1). Similar to the smoothing process discussed in the above paragraph, the average volume of the particles was estimated to be constant. Again, there were nearly no precursors left prior to the shape evolution from peanuts to dots. These facts imply that the formation of nearly monodisperse dots from the peanuts in Figures 2 is likely a continuation of the smoothing process discussed in the above paragraph, or intra-particle ripening.[36]

Elongated nanocrystals in other shapes were also observed in this non-injection system (see more results below). Upon annealing at the reaction temperatures, these elongated nanocrystals were all unstable. They became less and less sharp at corners, and eventually were converted to more or less dots. One additional example is provided in Figure S2, which illustrated the formation of nearly monodisperse rice, pearl-shaped rods, and the smoothing of the rods.

The results discussed in this sub-section revealed that elongated shapes are less stable in comparison to dots. Provided with sufficient time, the elongated nanocrystals would be converted to dots. This is qualitatively consistent with the semiconductor nanocrystal model systems studied previously, such as CdSe ones formed by hot-injection methods.[36] However, formation of monodisperse dot-shaped semiconductor nanocrystals from elongated ones has not yet been reported for those well-studied semiconductor nanocrystal systems, such as CdSe ones. This difference between the current system and the common semiconductor systems will be a topic in the Discussion.

Classic Ostwald ripening of monodisperse dot-shaped MnO nanocrystals was observed when the monodisperse dots were subjected to further heating. For example, the nearly monodisperse dots shown in Figure 1 were observed to undergo a classic Ostwald ripening process (Figure 3), from a monodisperse sample to a polydispersed one. As expected, the average volume of the nanocrystals evolved in a typical pattern for classic Oswald ripening process after the reaction proceeded for more than 30 min (Figure 3, top right).[37] The data points in the early stage, shorter than 30 min, did not follow the same linear trend (see the extended plot for this period of time in Figure 4d). This indicates the existence of a transition stage of Ostwald ripening, which includes the period of the formation of the monodisperse dots shown in Figure 1.

A quantitative analysis (Figure 4) of the reaction associated with the data shown in Figures 1 and 3 was performed. Details for the analysis are provided in the Experimental Section. The general assumption is that Mn atoms in the solution existed only significantly in the form of MnO nanocrystals and the carboxylate salt (see the last paragraph in the Discussion for justification). Thus, the monomer concentration (Figure 4a) was obtained

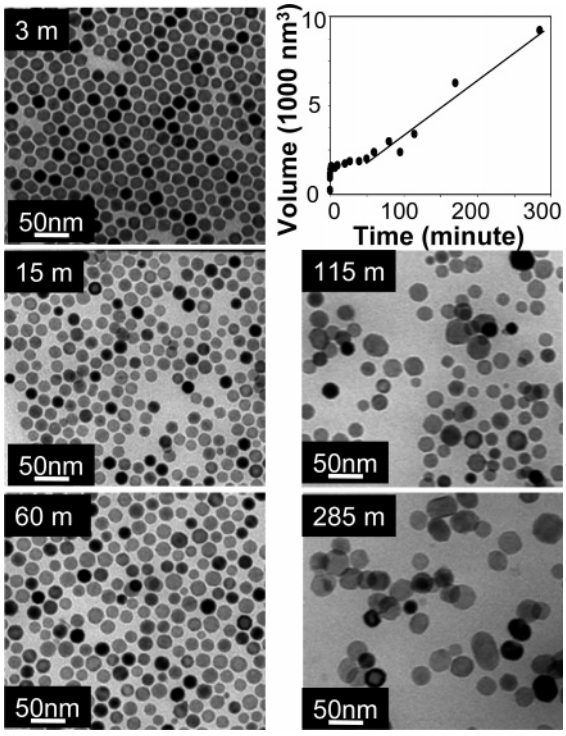

Figure 3. Classic Ostwald ripening of the nearly monodisperse MnO dots. See reaction in Figure 1.

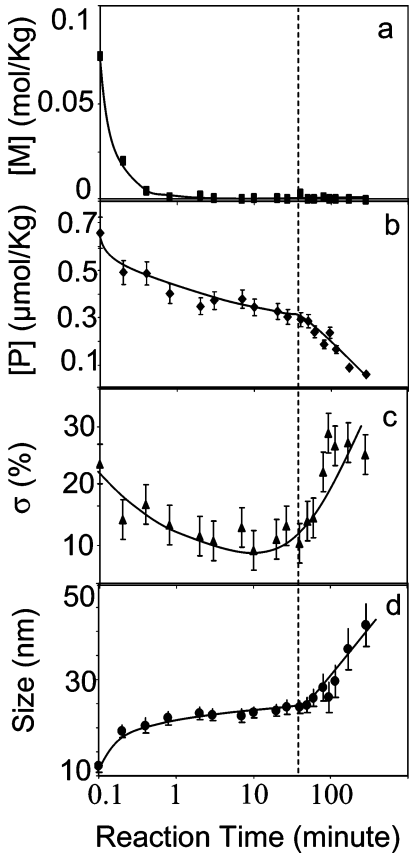

Figure 4. Quantitative results for the reaction associated with Figures 1 and 3. Note: The solid trend lines were added to guide the eyes. A dotted line was provided to indicate the starting point of classic Ostwald ripening.

by integrating the vibration band associated with the carboxylate salt centered at about 1556 cm^{-1} (see Figures 1 and 2). The average size (Figure 4d) and size distribution (Figure 4c) of

(36) Peng, Z. A.; Peng, X. *J. Am. Chem. Soc.* **2001**, *123*, 1389−1395.
(37) Lifshitz, I. M.; Slyozov, V. V. *J. Phys. Chem. Solids* **1961**, *19*, 35−50.

the nanocrystals were obtained by image analysis with about 400 particles for each point (see Experimental Section). The particle concentration (Figure 4b) was calculated using the amount of consumed monomers divided by the number of MnO units in an average sized nanocrystal at a given moment. Because TEM was used as the sole means for determining size and size distribution, it was difficult to evaluate particles smaller than about 2−3 nm. Consequently, it is impossible to study the nucleation stage quantitatively using this method.

The average size (Figure 4d) of the particles increased substantially in the very beginning (shorter than 1 min). The monomers were consumed rapidly in this rapid growth period (Figure 4d). This fast growth was followed by a slow growth period until the reaction proceeded for about 30 min, and then a rapid increase of the average size of the nanocrystals was observed in the classic Ostwald ripening discussed above (also see Figure 3, top right). Overall, the size distribution was narrowed down significantly in the first 10 min (Figure 4c), and then a significant broadening occurred after 30 min in the classic Ostwald ripening stage. For clarity, a straight dotted line was drawn in Figure 4 to indicate the beginning of the classic Oswald ripening.

A noticeable decrease of the particle concentration was observed in the entire duration of the reaction demonstrated here (Figure 4b), which indicates the entire process shown in Figure 4 was ripening in nature. Consistent with this, monomers were consumed almost completely in the very early period of this reaction (Figure 4a). As pointed out above, however, the average size of the nanocrystals kept increasing. This is also expected for a ripening reaction, although there are some substantial differences in size distribution evolution for the transient stage and the classic stage. Different from the classic Ostwlad ripening process (approximately after 30 min indicated by the dotted line in Figure 4), a continued narrowing of size distribution was observed in the transient stage of ripening, indicated by the decrease of the standard deviation of size distribution (δ) (Figures 4c and 1). Also consistent with a non-steady Ostwald ripening, the temporal evolution of the average volume of the nanocrystals did not follow the well-known linear relationship[37] (see Figure 3, top right, and the related text).

The evolution of size distribution profile of the MnO dots in the reaction related to Figures 1, 3, and 4 is also found to be consistent with narrowing of size distribution through a ripening process. The fundamental principle for ripening, no matter if it is in the transient stage or the late steady-state stage, is that the solubility of nanocrystals increases as the size of the nanocrystals decreases (see details in the Discussion). For the transient stage shown in Figure 4, the particle concentration decreased substantially. This decrease, according to the fundamental principle, should occur on the small size side, which is qualitatively consistent with the TEM images of the nanocrystals shown in Figure 1.

Quantitatively, this can be demonstrated through the size distribution evolution in the transient stage (Figure 5). The relatively broad size distribution at 0.8 min (Figure 4, bottom) was significantly narrowed as the reaction proceeded to 10 min (Figure 4, top). It should be pointed out that the overall size distribution for the sample at 10 min was the narrowest for this particular synthesis according to Figure 4c. The main change on the large size side was the increase of the population, but

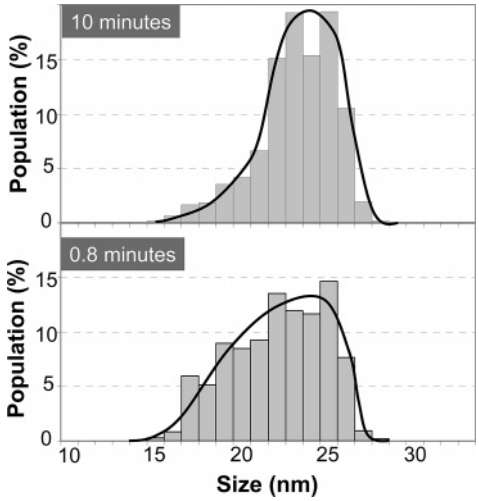

Figure 5. Size distribution histograms of MnO nanocrystals for two samples shown in Figure 4.

the population of the relatively smaller ones reduced dramatically. It is interesting to notice that both size distribution profiles in Figure 5 have a tail on the small size side, although this tail decreased significantly in the late stage. This distribution feature is qualitatively consistent with that expected for a ripening process.[37] A more detailed discussion about the size distribution evolution and narrowing of size distribution in this transient stage of ripening will be offered in the Discussion.

Ripening for the reactions with alcohol was a surprise to us. All original stearate ligands from $MnSt_2$ were converted into inactive esters before the ripening processes started (Figures 1 and 4a). In principle, both inter-particle and intra-particle ripening processes need the monomers to be reasonably soluble in the solution as it was discussed previously.[27] Consistent with this hypothesis, it was reported that, when alcohol was added and with similar reaction conditions, both ZnO and In_2O_3 nanocrystals did not show visible ripening.[27,28] Thus, one would not expect ripening to occur in the current system with a sufficient amount of alcohol added because alcohol consumed all active ligands, both stearates and stearic acid.

To clarify this confusing observation, MnO nanocrystals were isolated and purified from the reaction solution. These purified nanocrystals were added back into a controlled environment to study the ripening process. It should be pointed out that, although the vibrational band corresponding to carboxylate group at about 1556 cm^{-1} was barely observed in the unpurified reaction mixture (Figures 1 and 2), the purified nanocrystals showed a strong band in the region (Figure S3), indicating that the MnO nanocrystals were protected with stearate ligands, which is the same as that for the ZnO and In_2O_3 systems.[27,28]

The purified MnO nanocrystals were then subjected to annealing under different conditions. When they were heated in either pure ODE or ODE with alcohol, no significant change of the size and size distribution was observed. One example for these reactions is illustrated in Figure 6 (top). This indicates that alcohol on its own cannot initiate ripening.

The second set of experiments was performed with water-saturated Ar bubbling through the hot ODE solution of the purified MnO nanocrystals, instead of pure Ar flow. The other reaction conditions were maintained the same as those in the first set of experiments. This was achieved by bubbling the Ar

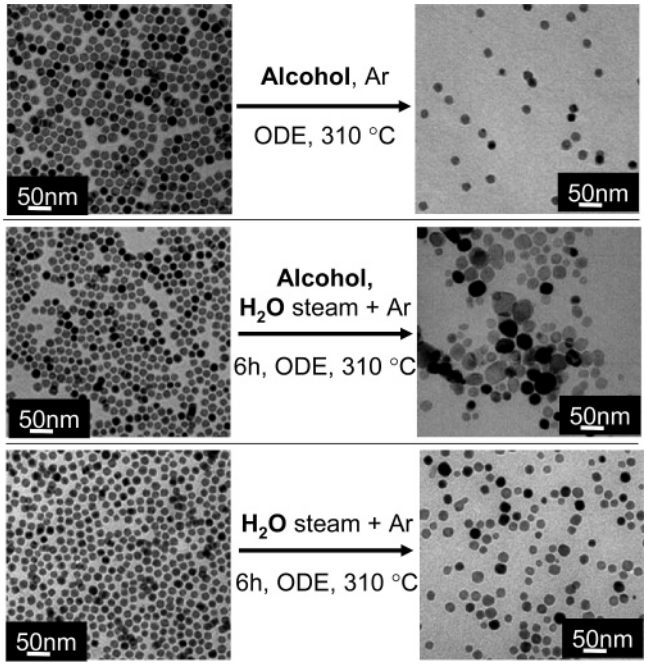

Figure 6. Ripening of purified MnO nanocrystals under different conditions.

gas through a liquid water reservoir, prior to being introduced into the reaction mixture. When the liquid water was at room temperature, no sign of ripening was observed.

However, when the liquid water in the reservoir was heated to boiling, ripening became immediately evident. Under otherwise the same conditions, the size distribution of the MnO nanocrystals became dramatically broadened when both alcohol and water steam were in place (Figure 6, middle). Even without alcohol, meaning purified MnO nanocrystals placed back in pure ODE, ripening of MnO nanocrystals was still observed as long as the water steam carried by Ar was bulbed into the reaction mixture (Figure 6, bottom).

The above results clearly indicate that water played a decisive role for any ripening process to occur in the current reaction system when alcohol was present. The substantial difference between bulbing Ar through room-temperature water and boiling water indicates that there must be a significant amount of water in the reaction system to take effect. This conclusion goes well with the reaction mechanism for the current system as to be discussed in the Discussion. Briefly, when alcohol was used, two stoichiometric amounts of water (measured by MnO unit) were yielded initially as a side product along the formation of MnO nanocrystals. The water consumed through ripening process was continuously regenerated in a ripening cycle.

Shape control of MnO nanocrystals has been a hot topic in the past few years, and some of the examples are cited in the references.[13,14,20−26] The current reaction system can also generate several different shapes with well-controlled size and shape distribution. Three-dimensional nanoflowers were reported separately,[38] and the related mechanism seems to be reasonably resolved, which will thus not be discussed here. The main focus of this Article is the mechanism on growth of dot-shaped nanocrystals and the related chemical reactions. The details of formation of the elongated nanocrystals are under study. Here, only some issues related to this work will be illustrated.

Figure 7 summarized a few typical examples of elongated MnO nanocrystals along with a monodisperse dot sample. The crystal structure of all of these shapes formed in the current reaction system was identified to be cubic MnO. One representative electron diffraction pattern is provided in Figure 7 (inset).

It was noticed that the purity of the $MnSt_2$ precursor played a visible role in determining the shape of the MnO nanocrystals and the reproducibility of the synthesis. If a stoichiometric amount of base was mixed with the fatty acid prior to the addition of $MnCl_2$, the resulting $MnSt_2$ (after purification and drying) was a white (or slightly pinkish) powder. If the reaction was with excess base, or, the base was added in after the mixing of the fatty acid and $MnCl_2$, the resulting fatty acid salts would be brown (see pictures in the Supporting Information, Figure S4). This brownish color was most likely associated with the formation of a small amount of Mn hydroxide or oxide. The existence of such impurities made the reaction to preferentially form elongated MnO nanocrystals with the same cubic structure, but the results were generally less reproducible. In addition to avoiding the preformation of Mn hydroxide and oxides,

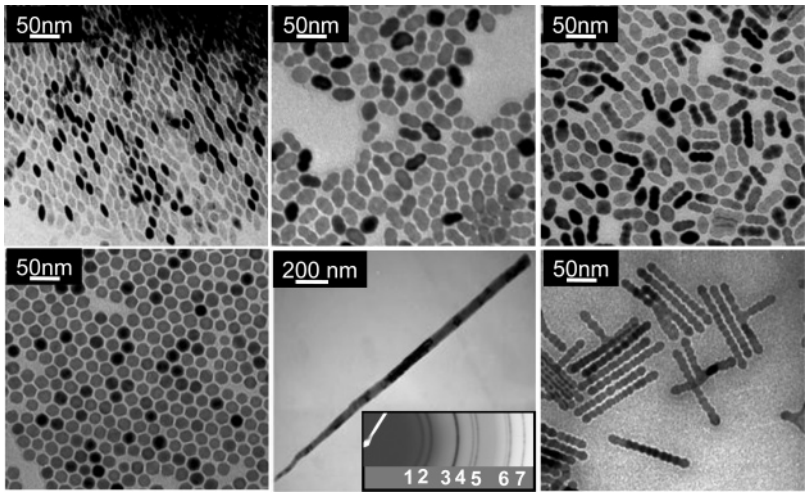

Figure 7. TEM images of differently shaped MnO nanocrystals with a representative electron diffraction pattern (inset). Spherical MnO nanocrystals were synthesized by a reaction of $MnSt_2$ with excess 1-octadecanol. Rice-shaped and other elongated MnO nanocrystals were synthesized by reactions of $MnSt_2$ with added free stearic acid. Rice-shaped MnO nanocrystals were formed at a very early stage. The indexes of the diffraction rings are as follows: (1) (111), (2) (200), (3) (220), (4) (311), (5) (222), (6) (420), and (7) (422). Note: The image of a long needle has a different scale bar.

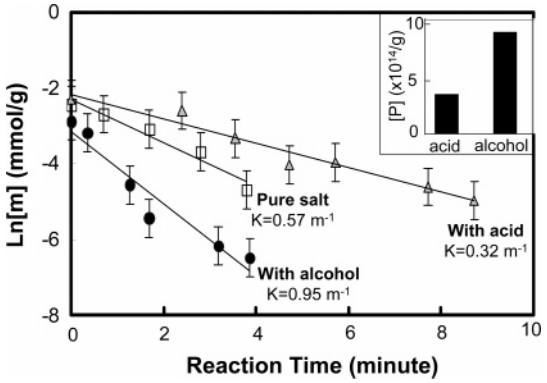

Figure 8. Temporal evolution of the monomer concentration under different reaction conditions determined by time-resolved FTIR measurements. Inset: Maximum particle concentrations for two reactions differed from each other by the addition of alcohol versus stearic acid.

methanol used as the solvent for the synthesis of $MnSt_2$ should also be removed by vacuum-drying. If methanol residual were left, the FTIR spectra would show the formation of ester even if no octadecanol, the activation reagents used exclusively in this work, were added. Again, precursors with methanol residual would also make the reactions less reproducible. It should be pointed out that, although the precursor purity played a role in determining the reproducibility and shape of the nanocrystals, the ripening patterns discussed above were found to be generally true.

Formation of elongated MnO nanocrystals followed the general trend observed for semiconductor nanocrystals, although no injections were involved in the current system. They were typically formed under the conditions with free stearic acid added. The existing theory[39] based on studies of the shape control of semiconductor nanocrystals indicates that, if the activity of the monomers is low, with stearic acid as inhibitors in the current case, the number of nuclei formed in the solution is small. Subsequently, a high remaining monomer concentration allows a small amount of nuclei to grow under an environment with high chemical potential, which makes the elongated nanocrystals stable and accessible in the reaction system. This rapid growth of the elongated nanocrystals depletes the monomer rapidly. As a result, the elongated nanocrystals are no longer stable, and intra-particle ripening[36] shall convert the elongated nanocrystals to more round in shape. As shown above, this model can well explain the results in the current system.

As discussed above, free ligands were frequently used for reducing the nucleus concentration in a system presumably by decreasing the reactivity of the monomers in the nucleation stage.[39] To our knowledge, this proposed reduction of the monomer reactivity has not yet been observed directly. Generally, the monomer concentration for semiconductor nanocrystals was calculated by the difference of the precursors added and the monomers in the form of nanocrystals for semiconductor nanocrystal systems.[36] Using the FTIR measurements, the precursor concentration in the current system can be directly measured. It thus offers an opportunity to confirm this important hypothesis.

Figure 8 illustrates the temporal evolution of monomer concentration of three reactions under identical conditions except the addition of inhibitor/activation reagents. One of the reactions had no inhibitor/activation reagent added, pure $MnSt_2$ in ODE. The second reaction had free stearic acid added as the inhibitor in addition to $MnSt_2$ and ODE. The third reaction was initiated with the addition of octadecanol as the activation reagents into the $MnSt_2$ and ODE mixture. For all three cases, the precursor concentration decreased as the reaction proceeded due to the formation and growth of the MnO nanocrystals (Figure 8). The depletion rate of the monomers, however, clearly differed from one case to another. The solid line for each case in the plot (Figure 8) is a fitting to the first-order of $MnSt_2$ concentration. The observed reaction constants are provided in the plot. Stearic acid, as expected for inhibitors, indeed decreased the reactivity of $MnSt_2$, about a 50% decrease under the current conditions judged by the reaction rate constants. Conversely, octadecanol as an activation reagent increased the reactivity of the $MnSt_2$ precursor about twice.

The theory of the shape-controlled growth of nanocrystals developed from the results on semiconductor nanocrystal systems further implied that the concentration of nuclei should be low for the formation of elongated nanocrystals in comparison to that for the formation of dots.[39] In the current system, and probably in other systems as well, it was difficult to exactly define the nucleus concentration. We suggest here to use the maximum particle concentration for a given reaction system as a measure of the nucleus concentration. The results shown in Figure 8 (inset) indicate that the nucleus concentration following this definition was about 2.5 times lower for the reaction with free stearic acid in comparison with that for the one with alcohol added. This further confirms the shape control model discussed above.

Discussion

"Focusing of size distribution" is currently the main model for explaining growth of nearly monodisperse nanocrystals with dot-shape.[10] To better understand the discrepancies between this existing model and the experimental results in this work, a brief discussion for the traditional "focusing of size distribution" model will be provided as follows.

The traditional "focusing of size distribution" requires that there should be no nucleation and all particles shall grow simultaneously in the duration of narrowing of size distribution in a reaction. The narrowing of size distribution occurs because the growth rate increases as the size of the nanocrystals decreases (Figure 9, left, and discussions below). This means that this pure growth stage allows the small nanocrystals to "catch up" with the large size nanocrystals.

The catching-up of the relatively small particles happens in a different way dependent on whether the reaction is diffusion-controlled or growth-controlled.[10] For growth-controlled systems, the smaller particles have a high reactivity because of their higher surface energy and relatively high surface to volume ratio. However, growth of high-quality nanocrystals has been mostly regarded as diffusion-controlled at present.[10] One of the main reasons is that the surface reaction sites of nanocrystals should be largely blocked by the ligands around each nanocrystal, which constitutes a good portion of the diffusion barrier. The dynamic feature of the surface ligands allows the diffusion through the ligand monomer to occur, but also spatially extends the size of the diffusion barrier. This feature justifies a diffusion

(38) Narayanaswamy, A.; Xu, H.; Pradhan, N.; Peng, X. *Angew. Chem., Int. Ed.* **2006**, *45*, 5361−5364.
(39) Peng, X. *Adv. Mater.* **2003**, *15*, 459−463.

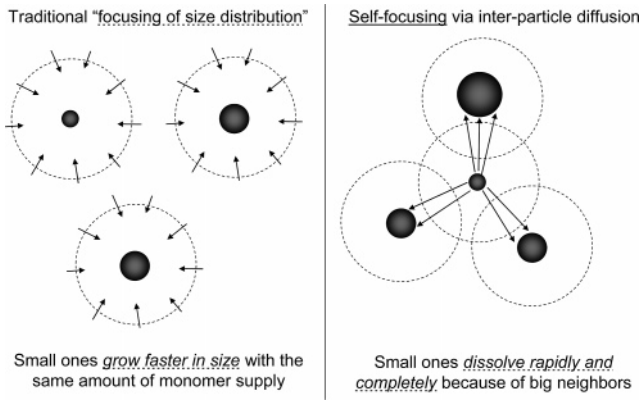

Figure 9. Differences between traditional "focusing of size distribution" (left) and self-focusing (right). The diffusion sphere for each nanocrystal is depicted as a dashed circle. The solid arrows represent the diffusion flux.

sphere model[2,40,41] as to be discussed below. For these reasons, the discussions below will be limited in the diffusion-controlled domain.

The growth rate difference between different size particles for a typical diffusion-controlled process can be approximately illustrated using the diffusion sphere model (Figure 9, left).[2,40,41] In this model, each nanocrystal should have a same sized diffusion sphere, and the size of the nanocrystal is negligible in comparison to the size of its diffusion sphere.[2,40,41] If the monomer concentration is sufficiently high, more or less the same amount of monomers should be diffused into the diffusion spheres in this simple picture (Figure 9, left), which should make the volume growth rate (V') of each nanocrystal the same.[2]

$$V' = {}^1/_2\pi d^2(d') = \text{constant} \qquad (1)$$

Equation 1 indicates that the size (d) growth rate (d') of nanocrystals, however, should dramatically increase as the size (d) of the nanocrystals decreases, proportional to $1/d^2$. This means that the relatively small nanocrystals shall rapidly catch up while all particles in the solution are growing simultaneously. In a mean field consideration, all small nanocrystals should grow rapidly and the small sizes in the initial size distribution profile should be "cut off", which results in a symmetric size distribution.

In summary, there are several interesting signatures for the traditional "focusing of size distribution" model. The first feature is that the particle concentration during "focusing of size distribution" should be a constant. The second feature requires that the monomer concentration in the solution must be sufficiently high and the monomers shall be significantly consumed due to the simultaneous growth of all nanocrystals. The third feature indicates that the size distribution profile of the nanocrystals should not develop a tail on the small size side. Evidently, numerous experimental results demonstrated in the Results were against all of these signatures of the traditional "focusing of size distribution".

To our knowledge, there was only one publication in the literature that reported the temporal evolution of particle concentration for non-injection-based systems,[16] which was based on the growth of CdSe nanocrystals in ODE and determined using the size-dependent optical properties of CdSe nanocrystals. Interestingly, it also revealed a substantial decrease of the particle concentration in the course of narrowing of size distribution. Unfortunately, the authors did not report the evolution of monomer concentration and the size distribution profile.

An alternative mechanism for the formation of monodisperse dots in these non-injection-based systems seems to be needed as the existing "focusing of size distribution" model is contradictory to the experimental results as discussed in the above section. A recent discovery, inter-particle diffusion with a high particle concentration, attracted our attention. This was observed by studying the dissolution/ripening processes of CdS and CdSe nanocrystals.[34] Under high particle concentrations, the complete dissolution of the small particles could occur rather rapidly through inter-particle diffusion. This greatly reduces the population of the relatively small particles in the solution, which is similar to what is illustrated in Figure 5. For pure dissolution/ripening processes studied for CdS nanocrystals, the size distribution could be narrowed down to a few percent range (about 7% for the example reported).[34] This value is much below the low limit of size distribution (about 25%) predicted by the recent theoretical treatments of classic Ostwald ripening in nanometer size regime.[41,42]

Although this inter-particle diffusion phenomenon was identified in dissolution/ripening of nanocrystals for pre-synthesized nanocrystals and mostly at room temperature, it may actually be more significant for a synthetic reaction under elevated temperatures. Typically, a synthetic system could have a high particle concentration, so inter-particle distance should be small. At a fixed particle concentration, as the thermal energy of particles increases, the frequency for the particles to encounter each other shall increase substantially.[43] This means that narrowing of size distribution enabled by inter-particle diffusion could occur in a synthetic system similar to the one studied here. Because this new size-focusing phenomenon occurs by simply mixing reaction components together, opposite to build-up of a nucleation-growth balance by hot-injections of the precursors,[2] we tentatively suggest to name it as "self-focusing of size distribution", that is, "self-focusing" in short. There is another important reason, to be discussed later, that promoted us to call this phenomenon self-focusing.

With the particle concentrations in this work, roughly close to 1 μmol/kg (Figures 4b and 8 (inset)), the average distance between particles would be about 100 nm. Thus, if the thickness of the diffusion sphere of each nanocrystal (roughly 20 nm in average) was greater than 50 nm, overlapping of the diffusion spheres of nanocrystals in the solution should become inevitable from a mean field standpoint, even if ignoring the vigorous thermal motion of the particles under elevated temperatures. As often cited in literature, the size of a particle has been regarded as negligible in comparison to the diameter of the diffusion sphere for diffusion-controlled growth.[2,40,41] It should be noticed such a consideration was originally proposed for the growth of nearly monodisperse colloidal particles in micron size range,[40] which should thus be quite valid for the discussions in nanocrystal systems. On the contrary, because the monomer concentration rapidly reached nearly zero (Figures 1 and 4),

(40) Sugimoto, T. *Adv. Colloid Interface Sci.* **1987**, *28*, 65−108.
(41) Mantzaris, N. V. *Chem. Eng. Sci.* **2005**, *60*, 4749−4770.
(42) Talapin, D. V.; Rogach, A. L.; Haase, M.; Weller, H. *J. Phys. Chem. B* **2001**, *105*, 12278−12285.
(43) Atkins, P. W. *Physical Chemistry*, 6th ed.; W. H. Freeman & Company: New York, 1998.

growth due to the solution−particle diffusion was insignificant shortly after a reaction was initiated. Therefore, the narrowing of size distribution of the dots should be largely due to self-focusing, instead of the traditional "focusing of size distribution".

Similar to any mechanism consideration for crystallization, the Gibbs−Thompson equation[44] (eq 2) is the starting point for describing self-focusing in non-injection synthesis.

$$S_d = S_\infty \exp(4\sigma V_m/dRT) \quad (2)$$

σ and V_m are the specific surface energy and molar volume of a crystal, respectively. S_∞ is the solubility of the bulk crystal, and S_d is that for a crystal with its diameter (or size) as d. R is the gas constant, and T is absolute temperature.

Equation 2 implies that the solubility of crystals decreases substantially as their size increases, which is a result of the decrease of the surface atom ratio.[8] The driving force for inter-particle diffusion is the solubility gradient between two nearby nanocrystals with their diffusion spheres overlapping with each other. Because the monomer concentration during the narrowing of size distribution observed in the current system was close to zero (see data in Figures 1 and 4), the solution−nanocrystal diffusion can be ignored. With these facts, one can then obtain eq 3.

$$d' = 5D\pi q^2(S_{ave} - S_d)[P] \quad (3)$$

where $S_{ave} - S_d$ is the mean inter-particle solubility gradient, D is the diffusion coefficient of monomers, q is the radius of the diffusion sphere, and [P] is the particle concentration. Considering the rapid thermal motion of the particles in the solution, each particle shall change its neighbors frequently. For this reason, the solubility of the neighboring nanocrystals for a given particle is represented by an ensemble averaged value, S_{ave}. The particle concentration, [P], appears in both eq 3 and the inter-particle diffusion term in the original equation.[34] This is because the number of neighboring particles and the average distance between the particles are both related to particle concentration.

Equation 3 tells that, if a particle is smaller than the average size, the growth rate shall be negative (dissolution). Conversely, for a particle larger than the average size, the growth rate is positive (growth). This means that, if a reaction is truly controlled by inter-particle diffusion, the relatively small particles shall always dissolve and their monomers will directly feed the growth of their neighboring big ones (Figure 9, right). This serves as the basis for narrowing the size distribution through two different pathways.

The first pathway lies on controlling the generation of new nuclei. If the system is truly controlled by inter-particle diffusion, a self-separation of nucleation and growth should be expected, which is different from the traditional "focusing of size distribution". By the initial nucleation of a large population of nanocrystals and the subsequent growth of these nanocrystals to relatively large sizes, monomer concentration should be rapidly depleted (see Figure 4a as an example). This shall slow down the nucleation rate. More importantly, the slowly formed nuclei, very small in size and highly soluble (eq 2), became extremely unstable and would be instantaneously consumed by the large amount of big particles in the surroundings through inter-particle diffusion (Figure 9, right). This means that the nucleation process would be practically stopped. This is the other reason why this alternative model might be called "self-focusing".

The second pathway is based on the exponential increase of the solubility of the nanocrystals as their size decreases (eq 2). This can be visualized by comparing the dissolution and growth rates of two particles: one is smaller than the mean size by Δd, and the other is greater than the mean size by Δd. Because of the exponential nature of the size dependence of the solubility of the nanocrystals in a solution (eq 2), the dissolution rate of the small nanocrystal should be substantially higher than the growth rate for the large nanocrystal (see eq 3). Furthermore, as dissolution/growth proceeds, this rate difference shall further be enhanced rapidly. This is the key reason why small nanocrystals, from either growth or nucleation, in a distribution can be dissolved rapidly and completely through self-focusing.

There is a pure geometric argument that also favors narrowing of size distribution under inter-particle diffusion. For instance, if all of the monomers of a 15 nm particle are transferred onto a 25 nm particle, the size of the 25 nm particle will only increase by about 6%. This means that, under the control of inter-particle diffusion, the particles smaller than the mean size in the solution shall dissolve very rapidly, without much size increase of the large particles. Even among the large particles with a positive growth rate defined by eq 3, this geometric argument shall still improve the size distribution because the relatively large ones shall grow slower with the same amount of feedstock. For instance, the monomers sufficient for a 25 nm particle to grow by 6% will be enough for a 20 nm particle to grow for about 20%. This indicates that, among the large particles with a positive growth rate, the large ones have a tendency to "wait for" the smaller ones to catch up.

It should be pointed out that self-focusing might not only be in place for non-injection-based synthesis. This is so because the particle concentration in some hot-injection systems was also found to decrease while the size distribution was narrowing down.[45] In addition, the nucleation process for injection-based methods often lasted for a significant amount of time, a few minutes,[45] which is not really instantaneous.

As the inter-particle diffusion proceeded, the particle concentration would eventually drop to a critical level, which makes inter-particle diffusion loss its dominating position. At this point, the classic Ostwald ripening through the traditional solution−particle diffusion would gradually kick in and become more and more dominating in the system (Figure 3 and the late stage in Figure 4). Consequently, the size distribution of nanocrystals broadened.

Formation of nearly monodisperse dots from elongated nanocrystals was an interesting observation. FTIR spectra indicate (Figure 2) that there was no net monomer consumption in the process, and the average volume of the nanocrystals judged by TEM (Figure 2) did not change significantly. These features match intra-particle ripening observed in the case of CdSe nanocrystals, which changed the CdSe nanorods to dots.[36] However, the intra-particle ripening observed for CdSe nanocrystals could only occur with a quite high monomer concentration, and the resulting dots were far from being monodisperse. The first difference was likely due to the vastly different

(44) Mullin, J. W. *Crystallization*, 3rd ed.; Butterworth-Heinemann: Oxford, 1997.

(45) Qu, L.; Yu, W. W.; Peng, X. *Nano Lett.* **2004**, *4*, 465−469.

solubility/stability of the metal complexes in each system. Because of the very low solubility of Mn ions in the current system, it was possible to have intra-particle ripening under a very low monomer concentration.

The outstanding size distribution of the dots formed by intra-particle ripening in the current system is also likely a result of the low solubility of $MnSt_2$ monomers. This means that the intra-particle ripening of the elongated nanocrystals could be well separated from the following classic Ostwald ripening that could only start with a very low monomer concentration. The low stability/solubility of the monomers in the solution made the intra-particle ripening last for a long period of time (Figures 2 and S2), a few hours. Consequently, if the volume distribution of the elongated nanocrystals were sufficiently narrow, a nearly monodisperse sample of dot-shaped nanocrystals would be the result (Figure 2). If the particle concentration were sufficiently high, a self-focusing process prior to the classic Oswald ripening may occur, which could further improve the size distribution of the dots.

The molecular mechanism of the current system can be reasonably identified because of its simplicity and all organic species are IR active. When heating $MnSt_2$ precursor in ODE, with or without free stearic acid (HSt) added, the precursor went for hydrolysis to yield MnO and HSt indicated by the increased (decreased) intensity of the corresponding $-COOH$ ($-COO^-$) vibration band (see FTIR spectra in Figure 2). Although zinc stearate did not go for any hydrolysis,[27] a similar process was identified for the formation of In_2O_3 nanocrystals.[28] The hydrolysis reaction is as follows:

$$MnSt_2 + H_2O \rightarrow (MnO)_n + HSt \quad (4)$$

Here, $(MnO)_n$ represents MnO nanocrystals. HSt, either generated by the above reaction or added as inhibitors, made the above reaction reversible.

$$(MnO)_n + HSt \rightarrow MnSt_2 + H_2O \quad (5)$$

The above chemical equations (eqs 4 and 5) should be the reactions involved in the formation of MnO nanocrystals without alcohol added (see Figure 2 as one example), with eq 4 for the growth and eq 5 for dissolution needed for any ripening process, that is, intra-particle ripening, self-focusing based on inter-particle diffusion, and the classic Ostwald ripening.

The reactions with octadecanol (ROH) added as activation reagents were quite different from the reactions discussed above. Alcohol reacted with $MnSt_2$ to form ester (see FTIR spectra in Figure 1), H_2O, and MnO nanocrystals.

$$MnSt_2 + 2ROH \rightarrow (MnO)_n + 2St{-}OR + H_2O \quad (6)$$

Different from the reaction in eq 4, the above reaction has been proven to be irreversible because of the high stability of the esters formed (St−OR) (Figures 1 and 6 (top)) as demonstrated in the ZnO and In_2O_3 nanocrystal systems.[27,28] As a result, there was no evidence for ripening for both ZnO and In_2O_3 nanocrystal systems when alcohol was added into the reaction systems.[27,28] Several types of ripening processes, self-focusing based on inter-particle diffusion and the classic Oswald ripening, did occur in the current system with an excess of alcohol. The tests summarized in Figure 6 reveal that water was playing a decisive role in these ripening processes of the current system. With the experimental results shown above, the following reaction occurred as the initial step for a ripening process. The free stearic acid generated by this reaction can then react with the relatively small nanocrystals and dissolve them following the same reaction shown by eq 5. Consequently, the regenerated $MnSt_2$ by eq 5 would grow back to a large nanocrystal in the solution to complete a ripening process through either eq 4 without alcohol (Figure 5, bottom) or eq 6 with alcohol (Figure 6, middle). Consistent with this hypothesis, FTIR measurements (Supporting Information, Figure S5) showed the gradual formation of esters in the ripening process with the existence of alcohol. This conclusion also explains why the ripening processes occurred much faster when both alcohol and water steam were in place (comparing data in Figure 6, middle and bottom panels).

The molecular mechanism discussed here offers a strong backup of the assumption that the Mn atoms should exist in the form of MnO nanocrystals or $MnSt_2$. This assumption was the basis for the calculation of monomer concentrations in the reaction solution using FTIR spectra of $MnSt_2$ (see Figure 4 and related text). Although alcohol and ODE could be potential ligands for Mn ions and Mn ions could also be reduced to Mn^0, these species would not be stable at all. This is so because all of these compounds would be much more reactive toward water in comparison to $MnSt_2$. As discussed above, the reaction environment in the current system was sufficiently active to hydrolyze $MnSt_2$ (eq 4) and stearate ligands on the surface of nanocrystals (eq 7). Therefore, although it is difficult to exclude those complexes as possible intermediates, a significant concentration of those complexes in the reaction solution would be unlikely.

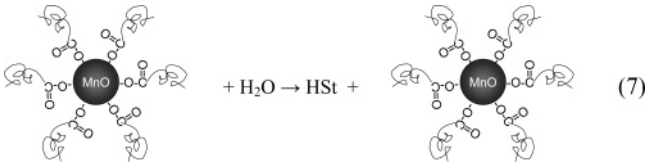

(7)

Conclusion

Quantitative results in this work indicate that a new mechanism for the formation of nearly monodisperse nanocrystals seems to exist. Different from the traditional "focusing of size distribution", the newly proposed mechanism, self-focusing, requires a reasonably high particle concentration but without the need of a high monomer concentration in the solution. With a high particle concentration, the diffusion spheres of nanocrystals shall overlap, which causes direct inter-particle diffusion from small particles to the relatively large ones. As a result, the relatively small nanocrystals in solution dissolve very rapidly and completely, which results in an automatic stop of nucleation and the cutoff of the very small nanocrystals in the distribution. The molecular mechanisms identified in this work implied that water actually played a critical role in both growth and ripening of the nanocrystals, although the reaction temperature was around 300 °C in a hydrocarbon solvent. The mechanistic information reported here shall not only assist development of relatively simple synthetic chemistry for high-quality nanocrystals with a variety of functions, but also impact other fields related to crystallization. This is so because quantitative studies of crystallization systems in nanometer regime are still rare in

the literature, which has been considered as the main roadblock for developing a meaningful theoretical framework for understanding crystallization.[44,46]

Experimental Section

Materials. Manganese chloride, stearic acid (95%), 1-octadecanol, 1-octadecene (ODE), methanol, and toluene were purchased from Aldrich and used as received without further purification. Tetramethylamonium hydroxide was from Alfa Asear.

Preparation of Manganese Stearate Precursor. Two methods were used to prepare manganese stearate. **Method A**: Manganese chloride and 2 equiv of stearic acid were dissolved in methanol solution, and the stearic acid was neutralized with equivalent tetramethylammoinum hydroxide in methanol solution. During the neutralization process, brownish $Mn(St)_2$ precipitated. $Mn(St)_2$ was washed with methanol three times and dried in a vacuum oven at 60 °C overnight. **Method B**: The stearic acid methanol solution was neutralized with tetramethyl ammonium hydroxide solution and then mixed with manganese chloride methanol solution. White $Mn(St)_2$ precipitated immediately after mixing. $Mn(St)_2$ was washed with methanol three times and dried in a vacuum oven at 60 °C overnight.

Synthesis of Dot-Shaped MnO Nanocrystals. $Mn(St)_2$ (0.5 mmol, white colored), 1-octadecanol (2 mmol), and ODE (5 g) were loaded in a 25 mL three-necked flask. The mixture was heated to 310 °C at a rate of 30 °C/min under Ar flow. The solution was kept at this temperature for a few hours. Aliquots were taken for FTIR and TEM analysis at different reaction intervals. The FTIR spectrum of the solution before reaction at room temperature was also taken as a reference for quantitative concentration calculation.

Synthesis of Peanut-Shaped MnO Nanocrystals and Shape Transition. $Mn(St)_2$ (1 mmol, brownish colored), 1 mmol of stearic acid, and 5 g of ODE were loaded in a 25 mL three-necked flask. The mixture was heated up to 300 °C at a rate of 30 °C/min. The solution was kept at this temperature for a few hours. Aliquots were taken for FTIR and TEM analysis. The FTIR spectrum of the solution before reaction at room temperature was also taken as a reference for quantitative concentration calculation.

First-Order Reaction Rate Determination. The $Mn(St)_2$ concentration in ODE was kept as constant (0.5 mmol of reactant in 5 g of solvent) for three reactions, pure $Mn(St)_2$, $Mn(St)_2$ plus free stearic acid (0.2 mmol), and $Mn(St)_2$ with 2 mmol of 1-octadecanol. The reaction conditions of these three reactions were the same as those described above. Five to seven aliquot solutions were taken during the first few minutes after the reaction reached the designated temperature, 310 °C. Sampling started at 290 °C when 1-octadecanol was used as activation reagent due to the very fast reaction rate. The FTIR spectrum of the solution before reaction at room temperature was also taken as a reference for quantitative concentration calculation.

FTIR Analysis and Temporal Concentration Calculation. FTIR spectra were recorded with a Bruker TGA-FTIR spectrometer. The samples for FTIR measurement were taken out of the reaction solution using a syringe, and, prior to any solidification of the reaction mixture, a thin film of a sample was then prepared on a CaF_2 salt plate for recording FTIR spectrum. The temporal concentrations of $Mn(St)_2$, stearic acid, and ester were calculated from integrated peak area of the corresponding peaks. The methyl group ($-CH_3$) peak at 1375 cm^{-1} was chosen as the reference peak for peak area calculations. The thickness of the thin films was controlled to avoid the saturation of any FTIR peak. The FTIR spectra of each sample were measured three times. The average concentration and standard deviation of these three measurements were calculated. The error bars represent three times of the standard deviation to achieve 95% confidence level.

Transmission electron microscopy images and SAED were taken on a JEOL 100 CX microscope. The MnO nanocrystals were dispersed in toluene to form an optically clear solution. A copper grid covered with a thin film of Formvar was dipped into the solution and dried in air. The size and size distribution of the nanocrystals for a given sample were initially determined using IMAGE J software. In each case, at least 2000 of particles were included for the statistics. However, this software was found to have quite low resolution, and the results were only used as references in semiquantitative evaluation. For the quantitative analysis shown in Figures 4 and 5, the results were based on the manual measurements of about 400 particles for each sample.

MnO nanocrystal concentration at a given reaction moment was determined by the combination of FTIR and TEM measurements. The concentration of the precursor, $Mn(St)_2$, at the given moment was determined by the corresponding FTIR spectrum as described above. The consumed concentration of Mn ions at the given moment was the difference between the initial $Mn(St)_2$ concentration and the $Mn(St)_2$ concentration at the corresponding moment. The average number of Mn ions in a single MnO nanocrystal was calculated using the average size determined with TEM and the density of MnO bulk crystal. The particle concentration of MnO nanocrystals in solution was then calculated by dividing the consumed Mn ion concentration by the number of Mn ions in a single MnO nanocrystal.

Acknowledgment. Financial support of this work was provided by the National Science Foundation.

Supporting Information Available: Supporting results mentioned in the text. This material is available free of charge via the Internet at http://pubs.acs.org.

JA073023N

(46) Peng, X. *Chem.-Eur. J.* **2002**, *8*, 334−339.